Gravity-mediated entanglement under local Gaussian control: existence, thresholds and experimental limits

Heah Hung Xun

22 August 2026

We ask whether two initially separable thermal mesoscopic masses in harmonic traps can develop non-zero *unconditional* entanglement through Newtonian gravity when the allowed controls are prescribed trap separation or trap-frequency changes, local continuous position measurement, Kalman–Bucy estimation and linear feedback. The model is the linearised two-mode Gaussian theory, with local Markov noise and no unlabelled non-local measurement or actuator. The answer is yes inside the model. A particularly transparent stable construction assumes a product thermal input of occupation $\bar{n}$, sets collinear geometry at $L/(2a) = 1.1$, and chooses $\kappa = (\omega_G/\omega_m)^2 = 0.5$, quench the gravitational curvature on, and read out after one relative-mode quarter-period. It gives $E_{\mathcal{N}}^{\max} = \max[0, \frac{1}{2} - \log_2(2\bar{n}+1)]$ bits, tolerates $\bar{n} < (\sqrt{2}-1)/2 = 0.2071$, and for fused silica requires $L/(2a) = 1.1$, $f_m = 108.19\,\mu\text{Hz}$ and $54.5\,\text{min}$ of coherent evolution. At $\bar{n} = 0.05$ the result is 0.3625 bits. The absolute effective temperature is only a few femtokelvin. Cooling and decompression to that unconditional resource are not demonstrated here. Correct secular rotating-wave analysis shows that a distance-modulated periodic steady state has limiting occupation 0.2071; the previously inferred divergent thermal tolerance arose from a fixed-purity formula applied to a damped oscillator. A full bare-local completely positive bath gives nearby but reservoir-dependent phase-resolved thresholds. Local measurement and classical feed-forward cannot create entanglement with gravity removed; a gravity-off positive result appears only if a dense feedback gain is inserted as an unnoised coherent interaction or an unphysical covariance is accepted. Thus there is no Gaussian no-go theorem against the ideal protocol. The obstruction is engineering: the mass-independent Newtonian curvature ceiling, sub-phonon preparation, multi-minute coherence at a microhertz trap, high detection efficiency, and finite-range stable actuation must all be met simultaneously.

1 The research question

The question is an existence question with an attribution condition. Starting from $\rho_A^{\text{th}} \otimes \rho_B^{\text{th}}$, does a stable control in the stated Gaussian class produce

$$\tilde{\nu}_- < \frac{\hbar}{2}, \qquad E_{\mathcal{N}} = \max\left[0, -\log_2\left(\frac{2\tilde{\nu}_-}{\hbar}\right)\right] > 0 \tag{1}$$

for the covariance averaged over all measurement records? Conditional entanglement is reported separately. Gravity must be the only non-local quantum interaction.

PROOF. Within the specified quadratic model the answer is yes: the finite-time quench constructed in Sec. 26 is stable and gives positive unconditional $E_{\mathcal{N}}$. SCALING ARGUMENT. No end-to-end parameter set in the audited sources simultaneously meets the required curvature fraction, occupation, clearance and coherence; this is a model- based engineering assessment, not a systematic survey of every levitated-mass platform.

2 Scope and assumptions

The in-scope state is Gaussian; the Hamiltonian is at most quadratic after a controlled Taylor expansion; measurements are local and linear; the estimator and actuator are linear; and environmental noise is Gaussian and Markovian. The sphere exterior field is Newtonian, the particles do not overlap, and the mechanical excursion is small relative to the centre separation. Prescribed $L(t)$ and $\omega_j(t)$ are classical controls. Their technical noise is parameterised but no detailed actuator is invented.

The main calculations use identical masses and traps. Unequal traps enter only where they separate the sum- and difference-frequency resonances. A completely positive amplitude- damping bath is used near the quantum regime; the momentum-diffusion Brownian model is used only for $\bar{n}_{\mathrm{th}} \gg 1$. Results that depend on the latter are marked as scaling arguments rather than microscopic predictions.

3 Source and notation audit

The Gaussian PPT certificate follows Simon [1], and the base-two logarithmic negativity follows Vidal and Werner [2]. The primary control sources are Poddubny *et al.* [3] and its stationary companion by Winkler *et al.* [4]. The central-force and gravitational context follows the independently read calculations of Kumar *et al.* [5] and Kumar and Paterek's unpublished supervisor-supplied working note [6], whose bibliographic year remains to be confirmed before external circulation. Kafri, Taylor and Milburn supply the measurement-channel control audit [7].

We use

$$\boldsymbol{u} = (x_A, p_A, x_B, p_B)^{\mathsf{T}}, \quad \sigma_{ij} = \tfrac{1}{2}\langle\{\Delta u_i, \Delta u_j\}\rangle, \quad \boldsymbol{\Omega} = \bigoplus_{j=A,B} \begin{pmatrix} 0 & 1 \\ -1 & 0 \end{pmatrix}. \tag{2}$$

Physicality is $\sigma + i\hbar\boldsymbol{\Omega}/2 \geq 0$, and partial transpose is $\Lambda = \mathrm{diag}(1, 1, 1, -1)$. Poddubny uses $\hbar = 1$, vacuum covariance $\mathbb{1}/2$ and natural logarithms; its negativities are divided by $\ln 2$ to obtain bits. The numerical covariance is rescaled symplectically to vacuum $\mathbb{1}/2$ before any eigendecomposition.

PROOF. A non-zero covariance cross-block denotes correlation, not entanglement. Equation (1), not the presence of a cross-block, is the certificate.

4 Exact Hamiltonian and the two geometries

For $V = C/s^n$, gravity has $C = -Gm^2$ and $n = 1$. The exact Hamiltonian is

$$H = \sum_{j=A,B} \left[\frac{p_j^2}{2m} + \frac{1}{2} m\omega_j^2(t) x_j^2 - f_j(t) x_j \right] + \frac{C}{s(t)^n}. \tag{3}$$

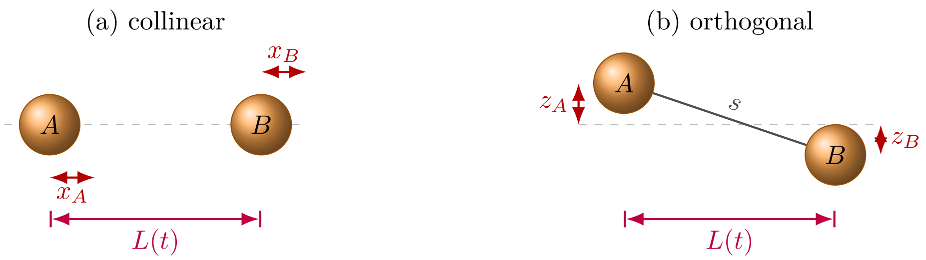

Figure 1: The two configurations. Collinear motion changes the separation to $s = L + x_B - x_A$ and has a linear force term. Orthogonal motion gives $s = [L^2 + (z_B - z_A)^2]^{1/2}$ and is even in the displacement. All labels are physical coordinates; the control is the trap-centre separation $L(t)$.

5 Quadratic expansion and its domain

With $r = x_B - x_A$,

$$V_\parallel = \frac{C}{L^n} - \frac{nC}{L^{n+1}}r + \frac{n(n+1)C}{2L^{n+2}}r^2 + O(r^3/L^{n+3}), \tag{4}$$

$$V_\perp = \frac{C}{L^n} - \frac{nC}{2L^{n+2}}r^2 + O(r^4/L^{n+4}). \tag{5}$$

The corresponding stiffnesses are $k_\parallel = n(n+1)C/L^{n+2}$ and $k_\perp = -nC/L^{n+2}$.

Proof. The exact Hessian is $\partial_i\partial_j(Cs^{-n}) = nCs^{-n-2}[(n+2)\hat{s}_i\hat{s}_j - \delta_{ij}]$. For gravity its eigenvalues are proportional to $(-2, 1, 1)$, proving the opposite signs and factor two without a coordinate convention. Numerical result. Finite differences reproduce the Hessian with relative Frobenius error 3.9×10^{-8}; independent polynomial fits recover the quadratic coefficients to 1.8×10^{-7} or better.

The covariance result is valid while the rms relative excursion and controlled sag are both small compared with L and with the surface gap. Near a soft-mode wall the excursion, not the algebraic symplectic eigenvalue, is the first validity test to fail.

For the constructive collinear benchmark, L is the *actual compensated equilibrium separation*: the local forces $f_A = -f_B$ in Eq. (3) cancel the Newtonian linear term at the expansion point. Without that compensation, the unshifted-trap sag at $\kappa = 0.5$ would be of order $L/2$ and the quadratic expansion would be invalid. Compensation removes the mean, but not force-noise, range or calibration requirements.

6 COM and relative variables

Define

$$R = \frac{x_A + x_B}{2}, \quad r = x_B - x_A, \quad P = p_A + p_B, \quad p = \frac{p_B - p_A}{2}. \tag{6}$$

Then $\{R, P\} = \{r, p\} = 1$, all cross brackets vanish, and

$$\sum_j \frac{p_j^2}{2m} = \frac{P^2}{2M} + \frac{p^2}{2\mu}, \quad M = 2m, \quad \mu = \frac{m}{2}. \tag{7}$$

Proof. The transformation is canonical but not orthogonal:

$$S\mathbf{\Omega}S^\mathsf{T} = \mathbf{\Omega}, \qquad \det S = 1, \qquad SS^\mathsf{T} = \mathrm{diag}(1/2, 2, 2, 1/2). \tag{8}$$

The relative frequency is

$$\Omega_\parallel^2 = \omega_m^2 + \frac{n(n+1)C}{\mu L^{n+2}}, \qquad \Omega_\perp^2 = \omega_m^2 - \frac{nC}{\mu L^{n+2}}. \tag{9}$$

7 Ground-state entanglement

For independent COM and relative ground states define $\gamma = \omega_m/\Omega$. Direct partial transpose gives

$$\tilde{\nu}_- = \frac{\hbar}{2}\sqrt{\min(\gamma, \gamma^{-1})}, \qquad E_\mathcal{N}(0) = \frac{1}{2}\left|\log_2 \gamma\right|. \tag{10}$$

Proof. Equation (10) follows both from the normal-mode covariance and from the block invariants. At non-zero coupling the ideal coupled ground state is entangled. For collinear gravity

$$\kappa = \frac{4Gm}{L^3\omega_m^2}, \quad \gamma = (1-\kappa)^{-1/2}, \quad E_\mathcal{N}(0) = -\frac{1}{4}\log_2(1-\kappa), \quad 0 < \kappa < 1. \tag{11}$$

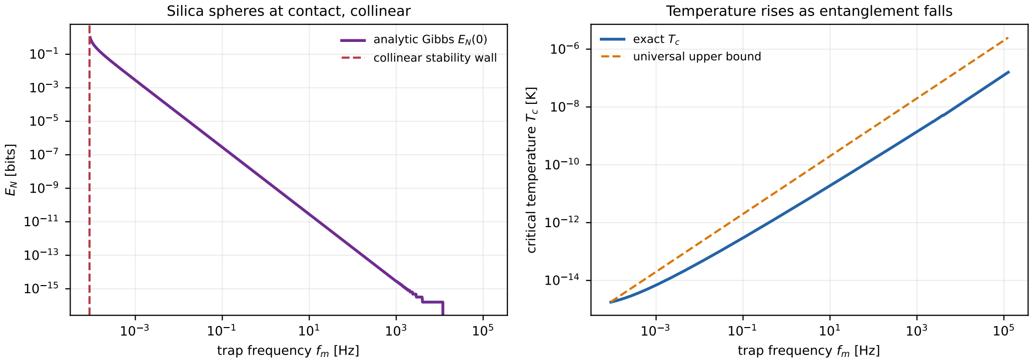

Figure 2: Analytical static trade-off at the limiting contact curvature of silica spheres. Left: ground-state logarithmic negativity and the collinear stability wall. Right: the exact Gibbs critical temperature and its universal analytical upper bound. The trap frequency is in hertz, $\rho = 2200\,\mathrm{kg\,m^{-3}}$, and $\lambda = 1$.

8 Thermal entanglement and critical temperature

Let $N_j = \coth(\hbar\omega_j/2k_BT_j) = 2\bar{n}_j + 1$. For a Gibbs state of the coupled Hamiltonian,

$$E_{\mathcal{N}} = \max\left[0, \frac{1}{2}\log_2 \frac{\max(\gamma,\gamma^{-1})}{N_{\mathrm{COM}}N_{\mathrm{rel}}}\right]. \tag{12}$$

For one temperature, T_c is the unique positive root

$$\coth\frac{\hbar\omega_m}{2k_BT_c}\coth\frac{\hbar\Omega}{2k_BT_c} = \max(\gamma,\gamma^{-1}). \tag{13}$$

Proof. With a_* defined by $\coth a_* = a_*$, $a_* = 1.199678640\ldots$, every branch obeys

$$k_BT_c \le \frac{\hbar\omega_m}{2a_*} = 0.416778\,\hbar\omega_m. \tag{14}$$

At weak collinear gravity, $T_c \simeq \hbar\omega_m/[k_B\ln(8/\kappa)]$. A classical high-temperature asymptotic is self-contradictory; the boundary is always in the quantum regime.

9 Coulomb versus gravity

Proof. At equal dimensionless γ, geometry, bath and control, Coulomb and gravity have identical linear Gaussian dynamics. Their experimental difference is the available curvature. For like charges,

$$\frac{|C_C|}{|C_G|} = \frac{k_eQ^2}{Gm^2}. \tag{15}$$

One elementary charge on each $1\,\mu\mathrm{m}$ silica sphere gives a curvature 4.07×10^{10} times gravity. At the Poddubny physical point ($50\,\mathrm{nm}$ radius, $L = 3.5\,\mu\mathrm{m}$, $f_m = 29.5\,\mathrm{kHz}$, ten charges), the equal-geometry orthogonal values are 0.011856 bits for Coulomb and 3.166×10^{-23} bits for gravity. The collinear counterparts are 0.022604 and 6.332×10^{-23} bits.

10 Product thermal state versus coupled Gibbs state

The commissioned initial state is a product of local thermal states. It is not the Gibbs state used in Eq. (12). If the static coupling is switched on suddenly, the COM mode remains stationary while the relative covariance breathes. At $t_q = \pi/(2\Omega)$,

$$E^{\mathrm{q}}_{\mathcal{N},\max} = \max\left[0, \frac{1}{2}\log_2 \frac{\max(\gamma,\gamma^{-1})^2}{N^2}\right]. \tag{16}$$

Proof. At zero temperature Eq. (16) is exactly twice the coupled-Gibbs negativity. The quench threshold is $N < \max(\gamma,\gamma^{-1})$, not $N^2 < \max(\gamma,\gamma^{-1})$.

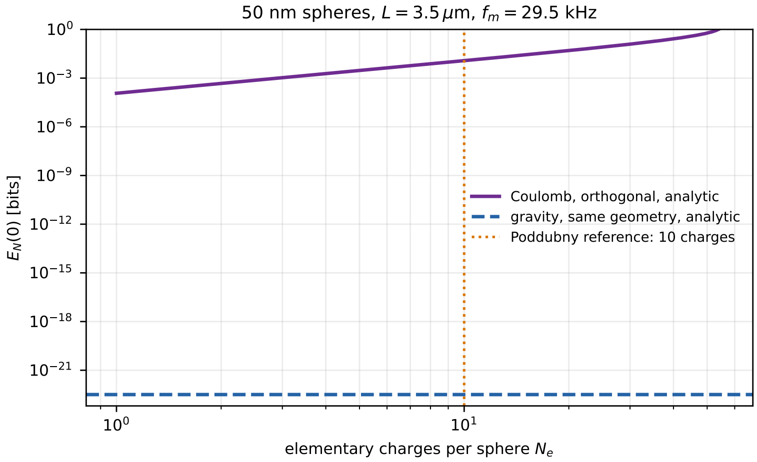

Figure 3: Analytical equal-geometry comparison at the Poddubny physical dimensions. The solid curve is orthogonal Coulomb coupling versus charge number; the dashed line is orthogonal gravity for the same mass, separation and trap frequency. The vertical line marks ten elementary charges.

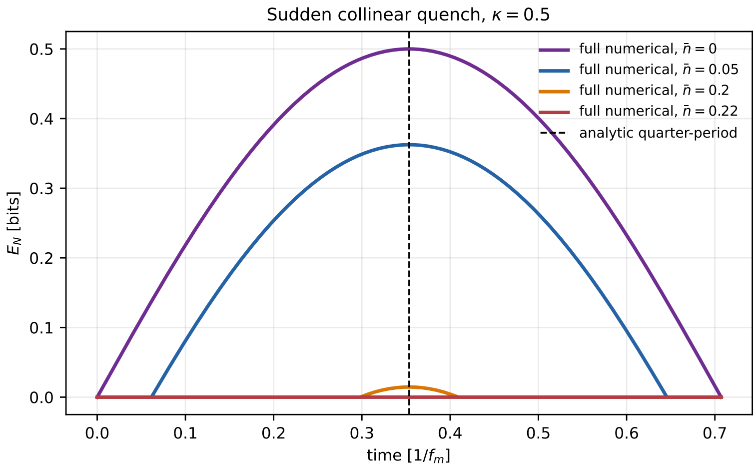

Figure 4: Full covariance evolution after a sudden collinear quench at $\kappa = 0.5$ for four initial occupations. Time is in trap periods $1/f_m$; the dashed line is the analytical relative-mode quarter-period. Curves are full numerical propagations and $E_{\mathcal{N}}$ is in bits.

11 Poddubny's orthogonal calculation

Poddubny uses transverse dimensionless quadratures $z_j = \sqrt{\hbar/(m\Omega_0)}X_j$ and obtains

$$\frac{H}{\hbar} = \frac{\Omega_0}{2}\sum_j (X_j^2 + P_j^2) + g_\perp(t)(X_A - X_B)^2, \quad g_\perp = -\frac{nC}{2m\Omega_0 L^{n+2}}. \tag{17}$$

The differential frequency is $\Omega_-^2 = \Omega_0^2 + 4\Omega_0 g_\perp$. Gravity therefore has $g_\perp = +Gm/(2\Omega_0 L^3)$ and stiffens the differential mode.

Proof. The source prints $g = C/(2nm\Omega_0 L^{n+2})$, wrong by $-1/n^2$ relative to the expansion. Fixed-g simulations survive; the microscopic map does not. At $g_0/\Omega_0 = 0.2$ the stated resonance is $2\sqrt{1.8} = 2.68328$, not 2.74.

12 The collinear counterpart

After shifting the static equilibrium, the same dimensionless Hamiltonian holds with

$$g_{\parallel} = \frac{n(n+1)C}{2m\Omega_0 L^{n+2}}, \qquad g_{G,\parallel} = -\frac{Gm}{\Omega_0 L^3} = -2g_{G,\perp}. \tag{18}$$

Thus collinear gravity is on Poddubny's negative-g softening branch despite the force being attractive. The geometry, not the everyday attractive/repulsive label, fixes the stiffness sign.

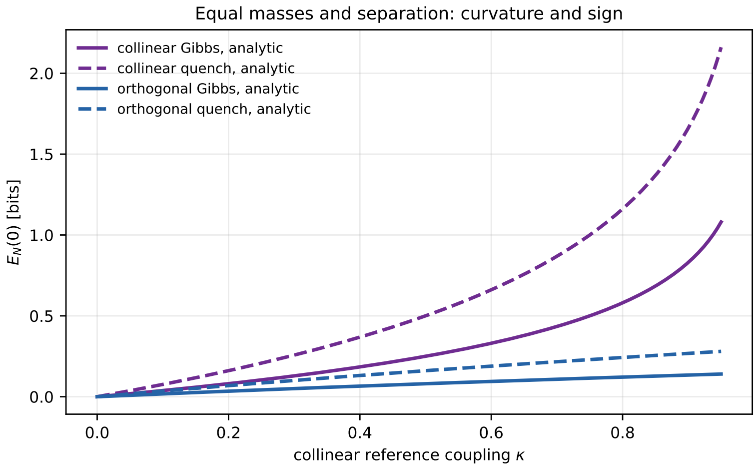

Figure 5: Analytical ground-state and quench negativities for equal masses and separation. The horizontal coordinate is the collinear reference κ; orthogonal curvature is half as large and has the opposite sign. Solid curves are Gibbs values and dashed curves are sudden-quench maxima.

13 Admissible controls and attribution

Admissible controls are prescribed local trap frequencies, a prescribed classical separation, local position records y_A, y_B, a Kalman filter, and forces applied locally. For the primary attribution calculation the measurement and actuation matrices are block diagonal across $A|B$. Cross-record classical feed-forward is analysed as a separate gravity-off audit, never folded silently into the gravitational result. Joint optical measurements, shared squeezed light, coherent controllers, correlated quantum forces and direct bilinear actuator Hamiltonians are outside this class.

Proof. This restriction is sufficient, not necessary: physically complete classical cross-feed-forward is LOCC and is also non-entangling. The block-diagonal primary class is chosen because it makes attribution transparent and prevents an incomplete feedback-noise model from masquerading as gravitational mediation.

14 Time-dependent distance modulation

Set

$$L(t) = L_0[1 + \eta_L \cos(\nu_d t)], \qquad L(t)^{-3} = L_0^{-3}[1 + \eta_L \cos(\nu_d t)]^{-3}. \tag{19}$$

For collinear gravity,

$$\Omega^2(t) = \omega_m^2 \left[1 - \kappa(1 + \eta_L \cos \nu_d t)^{-3}\right]. \tag{20}$$

At weak modulation, $\Omega^2(t) = \Omega_0^2[1 + h \cos \nu_d t]$ with $h = 3\kappa\eta_L/(1-\kappa)$ and closed-system amplitude exponent $s = \Omega_0 h/4$. Exact Fourier coefficients are used beyond $\eta_L = 0.2$ because the mean shift and second harmonic are then non-negligible.

Proof. Collinear modulation also drives a linear force proportional to $L(t)^{-2}$. It changes means only in the ideal centred covariance, but it is an actuator-range and technical-noise requirement absent in the orthogonal geometry.

15 Bogoliubov transformation derived

For the differential ladder operator a,

$$\frac{H_0}{\hbar} = Aa^\dagger a + \frac{B}{2}(a^2 + a^{\dagger 2}), \quad A = \Omega_0 + 2g_0, \quad B = 2g_0. \tag{21}$$

Let $b = a\cosh r + a^\dagger \sinh r$. The anomalous term vanishes when

$$\tanh 2r = \frac{2g_0}{\Omega_0 + 2g_0}, \qquad \Omega^* = \sqrt{A^2 - B^2} = \sqrt{\Omega_0^2 + 4\Omega_0 g_0}. \tag{22}$$

Proof. A real canonical transform exists iff $g_0 > -\Omega_0/4$, exactly the soft-mode stability condition. The driven operator obeys

$$2a^\dagger a + a^2 + a^{\dagger 2} = e^{-2r}(2b^\dagger b + b^2 + b^{\dagger 2}) + (e^{-2r} - 1), \quad e^{-2r} = \frac{\Omega_0}{\Omega^*}. \tag{23}$$

The drive is weakened on the stiffening branch and enhanced on the softening branch, but the formal divergence at instability lies outside the bounded-excursion model.

16 Interaction picture and rotating-wave selection

For non-degenerate local modes the position coupling contains

$$(a + a^\dagger)(b + b^\dagger) = ab + ab^\dagger + a^\dagger b + a^\dagger b^\dagger. \tag{24}$$

In the interaction picture these carry phases

$$ab : e^{-i(\omega_A+\omega_B)t}, \qquad a^\dagger b^\dagger : e^{+i(\omega_A+\omega_B)t}, \tag{25}$$

$$ab^\dagger : e^{-i(\omega_A-\omega_B)t}, \qquad a^\dagger b : e^{+i(\omega_A-\omega_B)t}. \tag{26}$$

Proof. Modulation at $\nu_d = \omega_A + \omega_B$ selects two-mode squeezing; at $\nu_d = |\omega_A - \omega_B|$ it selects a beam splitter. A passive beam splitter cannot entangle a product of thermal states, even at unequal temperatures. Degenerate traps make the sum resonance equivalent to squeezing the differential normal mode.

17 Full non-RWA Floquet dynamics

The full covariance obeys $\dot\sigma = A(t)\sigma + \sigma A^\mathsf{T}(t) + D$. Stability is decided by the spectral radius of the time-ordered monodromy. A periodic covariance is obtained from the discrete Lyapunov equation

$$\sigma_0 = M\sigma_0 M^\mathsf{T} + Q, \qquad Q = \int_0^\tau \Phi(\tau, t) D \Phi^\mathsf{T}(\tau, t)\, dt. \tag{27}$$

For quadrature damping $\Gamma = \gamma_m/2$ and $u = s/\Gamma < 1$, the correct open RWA variances are

$$V_-^{\mathrm{sq}} = \frac{N}{2(1+u)}, \quad V_-^{\mathrm{asq}} = \frac{N}{2(1-u)}, \quad V_+ = \frac{N}{2}. \tag{28}$$

Mixing the normal modes gives

$$\tilde\nu_- = \frac{N}{2\sqrt{1+u}}, \quad E_\mathcal{N}^{\mathrm{RWA}} = \max[0, \tfrac{1}{2}\log_2(1+u) - \log_2 N], \quad \bar n_* = \frac{\sqrt{1+u} - 1}{2}. \tag{29}$$

Proof. In this secular RWA reservoir the threshold tends to $(\sqrt{2}-1)/2 = 0.20710678$, not infinity. The discarded formula held the driven mode purity fixed while continuous diffusion increased it.

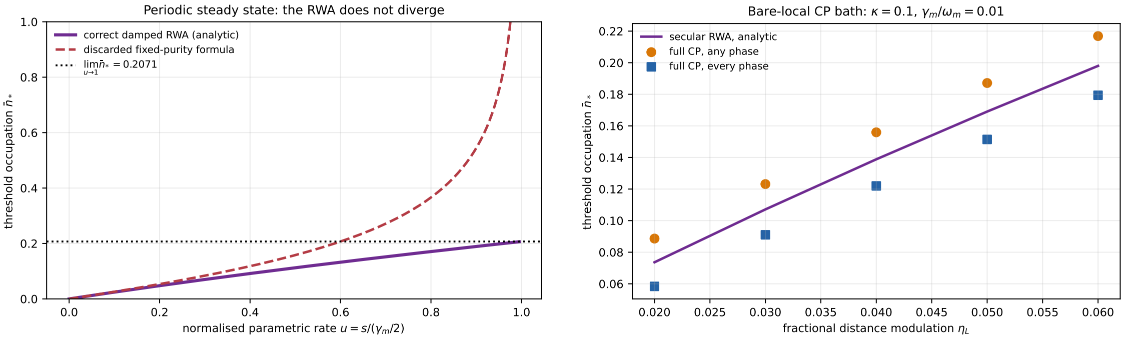

Figure 6: Left: analytical corrected damped RWA threshold against the discarded fixed-purity formula. Right: secular RWA (line) and full numerical Floquet–Lyapunov thresholds for independent bare-local completely positive amplitude damping at $\kappa = 0.1$ and $\gamma_m/\omega_m = 0.01$. Circles require entanglement at some phase; squares require it at every phase. Axes are dimensionless and $E_{\mathcal{N}}$ is evaluated in bits.

18 Open-system noise model

Near the ground state we use independent completely positive amplitude damping in each bare local trap basis,

$$A = A_H - \frac{\gamma_m}{2}\mathbb{1}, \qquad D_{\rm th} = \frac{\gamma_m}{2}(2\bar{n}_{\rm th}+1)\mathbb{1}, \tag{30}$$

with added recoil, imprecision-correlated and actuator diffusion declared separately. At high temperature and high Q, momentum Brownian diffusion $D_{pp} = \gamma_m(2\bar{n}_{\rm th}+1)$ is a useful scaling model.

Proof. A reservoir that damps the dressed normal modes is a different microscopic model: in bare local quadratures it is generally squeezed and correlated. The secular RWA limit in Eq. (29) and the full bare-local calculation must therefore not be identified beyond their common weak-coupling regime.

Proof. Momentum damping $-\gamma_m p$ with momentum-only vacuum diffusion is not a completely positive low-temperature channel. The inherited Kalman point that returned a small gravity-off $E_{\mathcal{N}}$ had $\nu = 0.49914 < 1/2$ and is rejected as unphysical.

Scaling argument. With $\gamma_m = \omega_m/Q$ and $k_BT \gg \hbar\omega_m$, a decoherence coefficient is $\Gamma_{\rm dec} \simeq 2k_BT/(\hbar Q)$. For weak collinear modulation,

$$\frac{s}{\Gamma_{\rm dec}} \mathit{simeq} \frac{3\eta_L \hbar Q \omega_G^2}{8k_BT\omega_m}. \tag{31}$$

This finite-pulse race is necessary and not sufficient; it does not replace the protocol-specific occupation threshold.

19 Kalman–Bucy estimation

The linear system and local record are

$$d\boldsymbol{u} = (A\boldsymbol{u} + B\boldsymbol{v})dt + d\boldsymbol{\xi}, \tag{32}$$

$$d\boldsymbol{y} = C\boldsymbol{u}\,dt + d\boldsymbol{w}, \tag{33}$$

with $\mathbb{E}[d\boldsymbol{\xi}d\boldsymbol{\xi}^{\mathsf{T}}] = Ddt$, $\mathbb{E}[d\boldsymbol{w}d\boldsymbol{w}^{\mathsf{T}}] = Rdt$ and $\mathbb{E}[d\boldsymbol{\xi}d\boldsymbol{w}^{\mathsf{T}}] = \Gamma dt$. The conditional mean and covariance obey

$$d\hat{\boldsymbol{u}} = (A\hat{\boldsymbol{u}} + B\boldsymbol{v})dt + K_f(d\boldsymbol{y} - C\hat{\boldsymbol{u}}dt), \tag{34}$$

$$\dot{\sigma}^c = A\sigma^c + \sigma^c A^{\mathsf{T}} + D - (\sigma^c C^{\mathsf{T}} + \Gamma)R^{-1}(C\sigma^c + \Gamma^{\mathsf{T}}), \tag{35}$$

$$K_f = (\sigma^c C^{\mathsf{T}} + \Gamma)R^{-1}. \tag{36}$$

Proof. The covariance equation is deterministic and contains no feedback gain. A linear force changes the conditional mean, not σ^c. Detection efficiency matters because back-action is paid in full while only a fraction of the record is recovered.

20 Linear feedback control

For $\boldsymbol{v} = -K\hat{\boldsymbol{u}}$, LQR minimises

$$\mathcal{J} = \int \mathbb{E}[\hat{\boldsymbol{u}}^\mathsf{T} P \hat{\boldsymbol{u}} + \boldsymbol{v}^\mathsf{T} R_u \boldsymbol{v}] dt. \tag{37}$$

The algebraic control Riccati equation fixes K. An energy cost cools local motion; an EPR cost suppresses the combinations that add excess noise to the desired correlations, as stressed by Winkler *et al.* [4].

PROOF. The separation principle permits estimator and regulator design separately, but it does not allow feedback to improve σ^c. Delay, saturation and actuator noise alter the excess covariance and closed-loop stability; they are not hidden inside an ideal gain matrix.

21 Conditional and unconditional covariance

Let $\Xi = \mathrm{Cov}(\hat{\boldsymbol{u}})$ over records. Orthogonality of the Kalman error and estimate gives

$$\sigma^u = \sigma^c + \Xi, \qquad \Xi \geq 0, \tag{38}$$

and, for time-independent matrices,

$$\dot{\Xi} = (A - BK)\Xi + \Xi(A - BK)^\mathsf{T} + K_f R K_f^\mathsf{T}. \tag{39}$$

PROOF. Partial transpose is a congruence and preserves Loewner ordering. The smallest symplectic eigenvalue is monotone under positive covariance addition, so $\tilde{\nu}_-(\sigma^u) \geq \tilde{\nu}_-(\sigma^c)$ and $E_\mathcal{N}^u \leq E_\mathcal{N}^c$. Conditional entanglement is therefore an upper bound, not a delivered unconditional state.

22 The gravity-off feedback audit

A physically complete controller that measures A and B locally, communicates the records classically and applies local conditional forces is LOCC. Kafri, Taylor and Milburn show explicitly that the measurement and fed-forward noise sit at the non-entangling boundary [7].

PROOF. With gravity off, local C makes σ^c a product covariance. Any dense classical gain changes only the distribution of conditional means, so

$$\rho^u = \int d\lambda \, p(\lambda) \, D_A(\lambda)\rho_A^c D_A^\dagger(\lambda) \otimes D_B(\lambda)\rho_B^c D_B^\dagger(\lambda) \tag{40}$$

is separable. A search over stable dense gains therefore gives $E_\mathcal{N}^u = 0$ when physicality is enforced.

An explicit counterfeit arises if the same dense gain is inserted directly into the operator drift as an unnoised spring. At gravity off, the artificial Hamiltonian $H_\mathrm{cf} = k_f(x_B - x_A)^2/2$ with $\kappa_f = 0.5$ has a quench maximum of 0.5 bit by Eq. (16). PROOF. This is a coherent non-local interaction, not measurement-record feedback. It is the gravity-off counter-example that the software audit must catch. Joint measurement or coherent feedback is likewise excluded unless it is named as the non-local resource.

NUMERICAL RESULT. An explicit physically complete gravity-off dense-gain test is stable with $\max \Re\lambda = -0.07107$ and has an unconditional cross-block element 1.25933, yet $\tilde{\nu}_-^u = 0.594330$ and $E_\mathcal{N}^u = 0$. The total-covariance construction and an independent eight-dimensional plant–estimator Lyapunov equation agree to 5.33×10^{-15}. Thus the requested counter-example search returns a negative physical result and a positive counterfeit only for the omitted-noise coherent spring.

23 Effective occupation and temperature

For a local one-mode block in its trap basis,

$$\bar{n}_E = \frac{1}{2}\left(\frac{\omega}{\omega_0}\sigma_{xx} + \frac{\omega_0}{\omega}\sigma_{pp} - 1\right), \qquad T_\mathrm{eff} = \frac{\hbar\omega}{k_B \ln(1 + 1/\bar{n})}. \tag{41}$$

Energy occupation and entropy-matched occupation differ for a squeezed state; both are reported when measurement produces local squeezing. In the ideal continuous-measurement limit the efficiency floor is

$$\bar{n}^{c}_{\min} \simeq \frac{1}{2}(\eta_d^{-1/2} - 1). \tag{42}$$

Scaling argument. Equation (42) implies $\eta_d > 50\%$ merely to cross the 0.2071 occupation ceiling, and substantially higher efficiency to leave robustness margin.

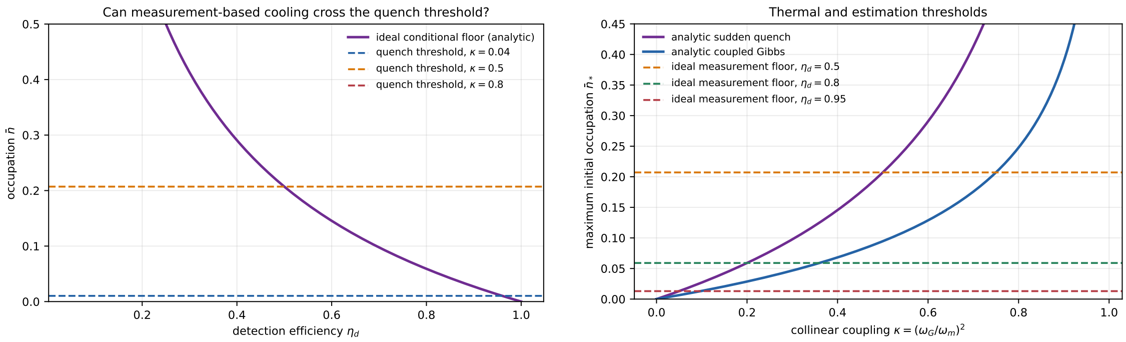

Figure 7: Analytical occupation requirements. Left: ideal conditional measurement floor versus efficiency and three quench thresholds. Right: Gibbs and quench occupation thresholds versus collinear κ, with three measurement floors. The figures compare occupation, not conditional and unconditional negativity.

24 Search over ten protocol families

The search uses the following explicit taxonomy, reconstructed because the inherited brief did not preserve a named list. "Local" means block-diagonal detector and actuator across the two masses.

Proof. There is no finite unconstrained optimum in this class. Arbitrarily strong local trap squeezing followed by any non-zero gravitational normal-mode phase difference can make $E_{\mathcal{N}}$ arbitrarily large while the gravity-off state remains separable. A claim of an "optimal Gaussian protocol" is therefore meaningful only after time, local squeezing, excursion and actuator bounds are declared.

Numerical result. The following table and finite-grid statements are numerical benchmark results, not class-wide optima. Under the benchmark caps $|\delta\omega_m^2|/\omega_m^2 \leq 0.02$, forty drive cycles and largest variance below three vacuum units, family 7 gives the largest finite-pulse value found in the bounded survey. At $\kappa = 0.1$ and $\bar{n} = 0.05$, a common trap-stiffness drive at $2\Omega_{\parallel}$ reaches a peak of 0.8466 bits and finishes at 0.8133 bits; the identical gravity-off local drive gives zero. Contact silica maps the pulse to 20.98 h, $T_{\text{eff}} = 4.40\,\text{fK}$ and $Q/T_{\text{env}} \gtrsim 2.0 \times 10^{17}\,\text{K}^{-1}$ for $D_{pp}t < 0.1$. It imports local non-classicality and is less gravity-dominant than the recommended quench.

Numerical result. A half-cosine interaction ramp never exceeded the sudden quench at matched final coupling: as $\omega_m \tau_{\text{ramp}}$ increases from 0 to 20, the peak falls from 0.3625 to 0.1143 bits, approaching the coupled-Gibbs value. A forty-cycle exact distance pulse at $\kappa = 0.1$, $\eta_L = 0.05$ and $\bar{n} = 0.05$ peaks at 0.6592 bits, but is an unstable finite pump rather than a periodic steady state. Combined distance and trap modulation can improve a fixed-duration point, yet the gain is phase sensitive and supplied mainly by the local trap drive.

Proof. A modulated separation cannot be centred at material contact. Non-overlap requires $L_0/(2a) \geq (1 - \eta_L)^{-1}$, reducing the mean contact-ceiling curvature by at least $(1 - \eta_L)^3$. The dimensionless contact-centred curves are therefore dynamical illustrations, not literal sphere trajectories.

No.	family	state reported	result within the model
1	coupled Gibbs, static	unconditional	Entangled below Eq. (12); tiny at ordinary traps.
2	sudden interaction/separation quench	unconditional	Exact constructive optimum Eq. (16).
3	finite separation ramp	unconditional	Interpolates between Gibbs loading and a quench; no larger robust maximum found.
4	finite resonant distance pulse	unconditional	Can accumulate squeezing; phase and excursion limited.
5	distance-modulated periodic state	unconditional	Stable for $u < 1$; secular-RWA ceiling 0.2071, with reservoir-dependent full thresholds.
6	trap-frequency decompression/quench	unconditional	Preserves occupation ideally and raises κ; duration and excursion costly.
7	sinusoidal trap-frequency drive	unconditional	Same parametric tongue, with modulated recoil and a physical phase.
8	combined separation/trap modulation	unconditional	Adds knobs but no thermal-threshold escape; more noise channels.
9	local measurement/Kalman preparation	conditional	Can prepare sub-phonon local states; never itself supplies unconditional entanglement.
10	local LQG plus gravitational evolution	unconditional	Approaches the conditional bound if efficiency, control and delay permit.

Table 1: The ten searched families and the covariance that is actually claimed. Dense cross-feedback is a gravity-off audit, not an eleventh admissible resource.

25 Numerical results

For non-overlapping spheres of density ρ at $L = 2\lambda a$,

$$\omega_G^2 = \frac{4Gm}{L^3} = \frac{2\pi G\rho}{3\lambda^3}. \tag{43}$$

Proof. Mass cancels. Contact silica gives $\omega_G/(2\pi) = 88.260\,\mu\text{Hz}$. At $f_m = 100\,\text{kHz}$, $\kappa = 7.79 \times 10^{-19}$, $E_{\mathcal{N}}(0) = 2.81 \times 10^{-19}$ bits and $T_c = 110\,\text{nK}$. The temperature is accessible only because it protects an immeasurably small entanglement.

At $\kappa = 0.5$ and $\bar{n} = 0.05$, analytical matched results are 0.1125 bits for the coupled Gibbs state, 0.3625 bits for the collinear quench, 0.02346 bits for the orthogonal quench, and 0.3255 bits for a periodic RWA state at $u = 0.9$.

Numerical result. A separate full laboratory-frame Kalman–feedback integration supplies a periodic existence point. It uses a sinusoidal collinear curvature with $\kappa = 0.4$, $g_1/\omega_m = 0.02$ (the first-order distance depth is $\eta_L = 0.1333$), local quantum-limited measurement $\Gamma_{\text{ba}}/\omega_m = 0.05$, unit efficiency, no unobserved diffusion and local cold damping $v_j = -0.5\hat{p}_j$. The largest closed-loop Floquet multiplier is 0.81666 for the full plant–estimator dynamics; the controlled-mean branch alone has multiplier 0.41662. Across a period the conditional negativity ranges from 0.3471 to 0.7204 bits, whereas the *unconditional* value ranges from 0.1541 to 0.5783 bits with mean 0.3893 bits. An initial product covariance $50\mathbb{1}$ converges to the same fixed cycle within 2.2×10^{-10} bits. An independent eight-dimensional augmented plant–estimator propagation agrees with the conditional-plus-excess covariance within 5.1×10^{-12} and with $E_{\mathcal{N}}$ within 1.8×10^{-11} bits. This is an existence result for the stated sinusoidal-curvature model; the exact $L(t)^{-3}$ waveform and a completely positive finite-temperature bath remain a robustness test, not an ingredient of the proof supplied by the finite-time quench.

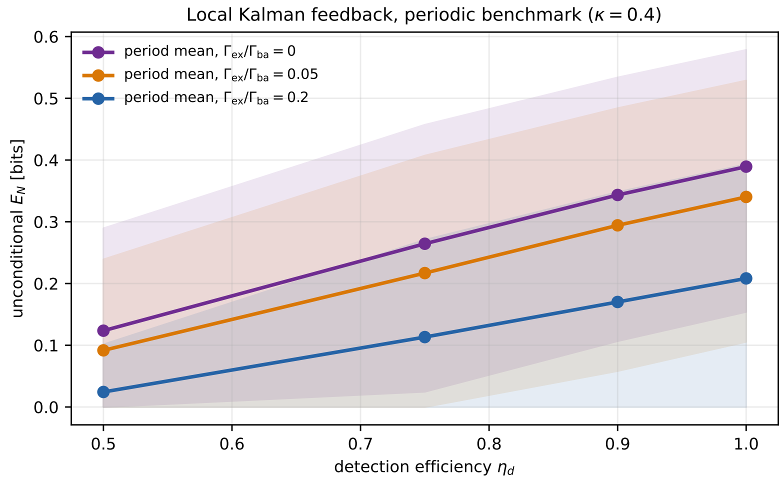

Figure 8: Full numerical periodic Kalman–feedback benchmark at $\kappa = 0.4$, $g_1/\omega_m = 0.02$, $\Gamma_{\mathrm{ba}}/\omega_m = 0.05$ and local gain $k_p = 0.5$. Lines are period-mean unconditional negativities versus detection efficiency; shaded bands span the minimum to maximum within a cycle. Colours denote unobserved momentum diffusion relative to measurement back-action. Every plotted covariance is physical and the controller is local.

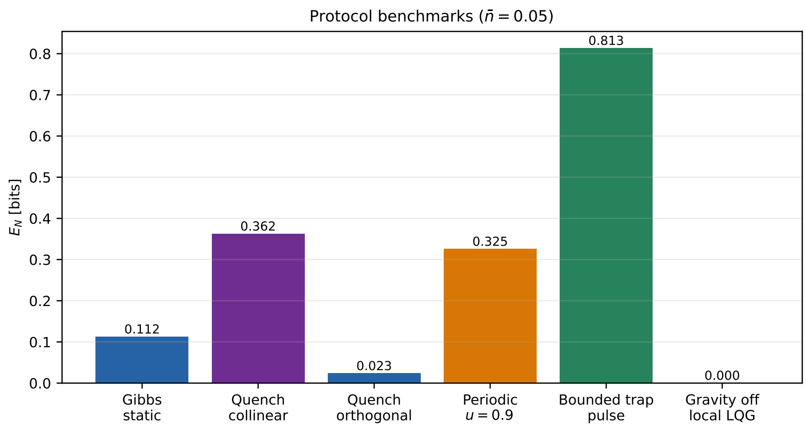

Figure 9: Protocol benchmarks at $\bar{n} = 0.05$. The first four bars use $\kappa = 0.5$; the periodic bar is the corrected RWA at $u = 0.9$. The bounded trap pulse uses $\kappa = 0.1$, $q = 0.02$ and forty cycles. The local-LQG gravity-off control is exactly separable. These bars compare different resources and do not imply equal actuator cost.

26 Recommended protocol

Proof. The constructive proof begins from an *assumed* unconditional product thermal covariance at the final trap frequency. It consists only of setting the finite- clearance geometry, quenching the gravitational curvature and evolving for one quarter- period. The following cooling and decompression steps are a conjectural implementation sketch, not part of that proof:

1. Conjecture. Cool two well-separated local traps to $\bar{n} \leq 0.05$ using local measurement and feedback. The ideal conditional floor reaches 0.05 only for $\eta_d > 1/1.1^2 = 0.8264$; a target $\eta_d \gtrsim 0.9$ leaves preparation margin. The unconditional feedback state, record-dependent means and residual squeezing remain to be verified directly.

2. Conjecture. Decompress while the masses are far apart so that the occupation, rather than the absolute temperature, is approximately preserved. No bounded low-noise schedule is supplied in this study.

3. Proof. Set collinear geometry at $L/(2a) = 1.1$ and $\omega_m = \sqrt{2}\,\omega_G(1.1)$, so $\kappa = 0.5$. Quench the gravitational curvature on faster than the relative period, compensate the deterministic mean force, and switch measurement light off if its recoil dominates.

4. Proof. Evaluate the unconditional covariance at $t_q = \pi/(2\Omega) = 3267.9\,\mathrm{s} = 54.5\,\mathrm{min}$.

For silica this uses $f_m = 108.19\,\mu\mathrm{Hz}$ and gives $E_{\mathcal{N}} = 0.36250$ bits at $\bar{n} = 0.05$; the zero-temperature value is 0.5 bit. The quench threshold is $\bar{n} < 0.20710678$, and $\bar{n} = 0.05$ corresponds to $T_{\mathrm{eff}} = 1.71\,\mathrm{fK}$ at the final trap frequency. This is an effective motional temperature after decompression, not a claim that a dilution refrigerator reaches femtokelvin.

For an explicit excursion check, take $a = 1\,\mu\mathrm{m}$ and $\rho = 2200\,\mathrm{kg\,m^{-3}}$. The surface gap is then 200 nm; the largest ideal relative rms fluctuation in the quench is 6.09 nm, or 3.05% of the gap. The quoted L is the force-balanced equilibrium separation. The unphysical $\lambda = 1$ contact limit is used only for curvature-ceiling plots, never as the constructive device. The abrupt interaction switch is an allowed prescribed-coupling idealisation; a finite-speed non-overlapping approach trajectory, force-compensation range and final tomography sequence remain unconstructed engineering requirements.

Numerical result. At this radius the mass is 9.22×10^{-15} kg and the static Newtonian force is 1.17×10^{-27} N. Without compensation it would displace each trap equilibrium by 275 nm; the mathematical benchmark assumes equal and opposite force compensation to retain the quoted centre separation. Three times the maximum rms relative fluctuation is 18.3 nm, 9.1% of the surface gap, and the cubic-to- quadratic Taylor ratio at that excursion is below 0.9%.

Numerical result. Direct 4×4 covariance propagation agrees with Eq. (16) to 2.1×10^{-15} bits at this point and passes the uncertainty test. Conjecture. A bounded shortcut-to-adiabaticity may make the decompression stage shorter, but its excursion, frequency range and added noise have not been demonstrated for this device.

27 Robustness and performance requirements

Timing error enters quadratically around the quarter-period; occupation error enters linearly through $-\log_2(2\bar{n} + 1)$; and the soft-mode excursion grows as $(1 - \kappa)^{-1/4}$. The recommended $\kappa = 0.5$ is deliberately away from the instability wall. Orthogonal geometry is always statically stable but gives substantially less entanglement at equal separation.

In the project's high-temperature covariance convention, $D_{pp} \simeq 2k_BT/(\hbar Q)$. Direct noisy covariance propagation at the recommended point gives

$$\frac{Q}{T_{\mathrm{env}}} > 4.89 \times 10^{16}\ \mathrm{K}^{-1} \tag{44}$$

for no more than a ten-per-cent reduction of the ideal negativity. The PPT survival boundary is $4.17 \times 10^{15}\,\mathrm{K}^{-1}$. For $Q = 10^9$ these correspond to $T_{\mathrm{env}} < 20.4\,\mathrm{nK}$ and 240 nK, respectively. The factor of two is fixed by defining the rate as D_{pp} rather than $\gamma_m\bar{n}$.

Scaling argument. The same two budgets are, respectively, $D_{pp} < 5.35 \times 10^{-6}\,\mathrm{s}^{-1}$ and $6.27 \times 10^{-5}\,\mathrm{s}^{-1}$, or single-oscillator heating below 0.231 and 2.71 quanta per day. With the one-sided convention $S_F^{(1)} = 2\hbar m \omega_m D_{pp}$, the corresponding white force-noise amplitudes are 8.41×10^{-29} and $2.88 \times 10^{-28}\,\mathrm{N\,Hz^{-1/2}}$. These conversions do not assert that gas, charge, trap-centre and recoil noise are actually white Brownian channels.

Proof. For $\bar{n} = 0.05$ the ideal quench remains entangled when the total collinear curvature fraction exceeds $\kappa_{\mathrm{crit}} = 1 - (2\bar{n} + 1)^{-2} = 0.17355$. The Newtonian cross-spring at the benchmark is $1.06 \times 10^{-21}\,\mathrm{N\,m^{-1}}$; a gravity-off background-gradient control must bound any unmodelled entangling cross-spring below $3.70 \times 10^{-22}\,\mathrm{N\,m^{-1}}$ merely to exclude a background-only false positive. More stringent calibration is required for a quantitative gravity claim.

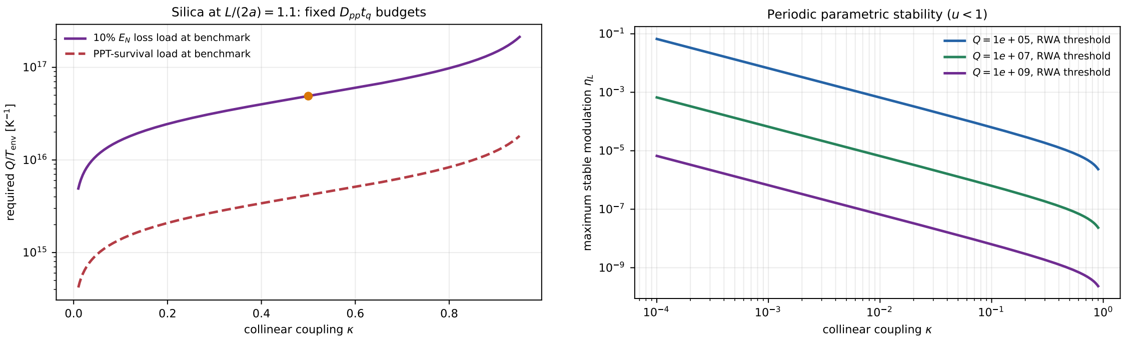

Figure 10: Scaling requirements. Left: Q/T_{env} for one quench quarter-period in silica at $L/(2a) = 1.1$ for two fixed $D_{pp}t_q$ budgets; their labels are calibrated at $\kappa = 0.5$, $\bar{n} = 0.05$. Right: leading RWA maximum stable distance modulation versus κ for three mechanical quality factors. Near the periodic wall the occupation ceiling saturates while excursion diverges.

Numerical result. For the full bare-local CP periodic test at $\kappa = 0.1$ and $\gamma_m/\omega_m = 0.01$, the thresholds are

η_L	any phase	every phase	secular RWA
0.02	0.08864	0.05837	0.07363
0.03	0.12315	0.09102	0.10711
0.04	0.15592	0.12198	0.13884
0.05	0.18714	0.15142	0.16906
0.06	0.21687	0.17939	0.19798

Direct occupation bisection and exact covariance scaling agree within 7.8×10^{-13}. The any-phase values exceed the secular-RWA values by 0.0150–0.0189 because bare-local and dressed-mode reservoirs are not the same bath. Thus finite saturation survives, but 0.2071 is not a bath-independent full-dynamics ceiling.

Numerical result. In the feedback-assisted periodic benchmark, entanglement at every phase requires $\eta_d \gtrsim 0.710$ with no extra diffusion and $\eta_d \gtrsim 0.791$ when $\Gamma_{\mathrm{ex}}/\Gamma_{\mathrm{ba}} = 0.05$. At unit efficiency the all-phase noise threshold is 0.16770. At one optimally chosen fixed phase per cycle it is 0.77014; at the arbitrary phase-zero boundary it is only 0.46692. A first-order causal delay model with fixed gain remains stable to $\tau\omega_m = 1.5616$; performance is non-monotone before that wall, so the stability boundary is more meaningful than a blanket delay penalty. At the silica contact-curvature ceiling the same benchmark maps to $f_m = 0.140\,\mathrm{mHz}$ and an ideal parametric build-up time of order 16 h. With the high-temperature Brownian conversion, all-phase periodic entanglement requires $T_{\mathrm{env}}/Q < 2.81 \times 10^{-17}\,\mathrm{K}$; at $Q = 10^9$ this is $T_{\mathrm{env}} < 28.1\,\mathrm{nK}$. The corresponding optimally phased once-per-cycle limits are $1.29 \times 10^{-16}\,\mathrm{K}$ and 129 nK. Recoil and actuator noise consume the same unobserved diffusion budget.

28 The answer

PROOF. A stable protocol with non-zero unconditional entanglement exists in linearised Gaussian Newtonian dynamics. Equation (16) and the operating point in Sec. 26 are a constructive proof. No measurement or non-local feedback is needed to create the covariance; local control is used only for preparation and mean stabilisation.

NUMERICAL RESULT. No searched family produces unconditional $E_{\mathcal{N}} > 0$ while also satisfying a complete device-level preparation, trajectory, force-background and readout specification. The recommended quench and secular distance-modulation protocol require sub-phonon input; local trap-frequency squeezing can trade additional local non-classicality, time and excursion for thermal tolerance, so no class-wide occupation ceiling exists without resource bounds. At the explicit 100-kHz benchmark the ideal gravitational negativity is of order 10^{-19} bits.

SCALING ARGUMENT. The limiting quantity is the mass-independent curvature

$$\omega_G^2 = \frac{2\pi G\rho}{3\lambda^3}. \tag{45}$$

For the recommended quench, the simultaneous requirements are an order-unity fraction of this curvature, $\bar{n} < 0.2071$ (preferably < 0.05), ideal detection efficiency above 82.6% if measurement preparation is attempted and preferably 90%, Q/T_{env} above 10^{15}–$10^{17}\,\text{K}^{-1}$, multi-minute stable actuation and small relative excursion.

PROOF. This is not a fundamental Gaussian no-go theorem. It is an engineering limitation of extraordinary severity. The threshold is crossed by lowering the final trap to order ω_G, preserving low occupation during decompression, and maintaining coherence for a relative quarter-period. Increasing mass at fixed density and fractional gap does not cross it.

29 Limitations and extensions outside the class

The quadratic model omits finite-size multipoles for non-spherical objects, anharmonic traps, surface forces, Casimir and patch potentials, separation-actuator noise, calibration drift, non-Markovian gas collisions, optical cavity modes and readout verification. Contact means centre separation $2a$, not material contact without surface clearance. A real device must bound every non-gravitational force gradient below the Newtonian one or calibrate it independently.

Gaussian dynamics cannot exploit non-Gaussian initial states, photon counting, nonlinear feedback, heralding or error-corrected encodings. Those resources can change witnesses and thermal robustness, but a joint measurement or shared quantum field is itself a non-local resource and changes the mediation claim. Recent work also stresses that conclusions about "classical gravity" depend on the model class [8]; for Wigner-positive Gaussian inputs and a quadratic potential the quantum and classical phase-space evolutions can coincide. Positive Gaussian $E_{\mathcal{N}}$ here is therefore a statement about gravity-mediated state entanglement within the quantum model, not by itself a witness that gravity is quantised. Wigner-negative inputs or cubic and higher gravitational terms are possible discriminating extensions, outside the present proof. This report makes no claim about all classical gravitational theories.

CONJECTURE. Local non-Gaussian preparation may reduce the required occupation or readout burden, but we have not found a verified treatment that removes the curvature ceiling for this harmonic two-mass geometry.

30 Next steps and reproducibility

The next experimental-theory calculation should optimise a bounded decompression schedule under an explicit actuator and excursion constraint, then include a cavity or free-space measurement model with recoil, efficiency, delay and saturation. A gravity-off run, an orthogonal-geometry run and a deliberately injected coherent cross-coupling are mandatory controls. It must also publish a numerical budget for Casimir, patch-charge and trap-force gradients relative to the Newtonian Hessian, plus a finite-duration unconditional covariance tomography protocol. The final observable should be an experimentally reconstructible PPT witness with calibration uncertainty, not only a model covariance.

All plotted data are regenerated by `code/gmec_generate_figures.py`; exact high-precision quench tables are generated by `code/gmec_protocol_search.py`; geometry, modulation, static and Kalman audits have separate scripts and reading notes. Numerical covariances are rescaled to vacuum $\mathbb{1}/2$; calculations below $\kappa = 10^{-16}$ use 60-digit arithmetic. The validation list is given in Appendix D.

A Long algebra for the partial transpose

In the laboratory basis write $\sigma = \left(\begin{smallmatrix} A & C \\ C^{\mathsf{T}} & B \end{smallmatrix}\right)$ and $\tilde{\Delta} = \det A + \det B - 2\det C$. Then

$$\tilde{\nu}_{\mp}^2 = \frac{\tilde{\Delta} \mp \sqrt{\tilde{\Delta}^2 - 4\det\sigma}}{2}. \tag{46}$$

For independent COM and relative thermal covariances, substitution and cancellation give

$$\tilde{\nu}_{\mp} = \frac{\hbar}{2}\sqrt{N_{\mathrm{COM}} N_{\mathrm{rel}}}\left\{\max(\gamma, \gamma^{-1})^{\mp 1/2}\right\}. \tag{47}$$

For the quench, the relative covariance after time t is

$$\sigma_r(t) = S_r(t)\sigma_r(0)S_r^{\mathsf{T}}(t), \quad S_r(t) = \begin{pmatrix} \cos\Omega t & (\mu\Omega)^{-1}\sin\Omega t \\ -\mu\Omega\sin\Omega t & \cos\Omega t \end{pmatrix}. \tag{48}$$

At $\Omega t = \pi/2$ the frequency mismatch enters twice, producing Eq. (16).

B Notation dictionary

Object	Poddubny	internship presentation	this report
coordinate	transverse dimensionless X_j	collinear physical x_j	physical x_j, geometry tagged
COM/relative	$X_\pm = (X_A \pm X_B)/\sqrt{2}$	R, r, P, p	R, r, P, p dimensionful
trap frequency	Ω_0	ω_m	ω_m
relative frequency	Ω_- or Ω^*	Ω	$\Omega_{\parallel,\perp}$
quadrature scale	$\sqrt{\hbar/(m\Omega_0)}$	rms spread $\sqrt{\hbar/(2m\omega_m)}$	names kept distinct
coupling	printed $g = C/(2nm\Omega_0 L^{n+2})$	signed C	direct Hessian; κ for gravity
vacuum covariance	$\mathbb{1}/2$	dimensionful	dimensionful; rescaled $\mathbb{1}/2$
negativity	$-\ln(2\tilde{\nu}_-)$, nats	base two	base two, Eq. (1)

C Parameter table

quantity	ordinary benchmark	constructive benchmark	meaning
ρ	$2200\,\mathrm{kg\,m^{-3}}$	same	fused silica
λ	1	1.1	contact ceiling / constructive clearance
f_m	100 kHz	108.19 µHz	final trap frequency
κ	7.79×10^{-19}	0.5	curvature fraction
$\bar{n}$	not fixed	0.05	initial local occupation
η_d	not fixed	target ≥ 0.9	detection efficiency
t_q	2.5 µs	3267.9 s	relative quarter-period
$E_{\mathcal{N}}^{\mathrm{q}}$	5.6×10^{-19} bits	0.3625 bits	ideal quench maximum

Table 3: Ordinary and finite-clearance constructive benchmarks; the latter is mathematically entangling but experimentally extreme.

D Validation tests

1. Symbolic Hessian, finite differences and potential regression agree on geometry.
2. Direct partial-transpose eigenvalues and block invariants agree on $E_{\mathcal{N}}$.
3. Randomised static checks cover both γ branches and unequal temperatures.
4. Quench propagation agrees with Eq. (16) on both branches.
5. Floquet exponents are checked by time-ordered monodromy and direct covariance growth.
6. Periodic covariances are checked by discrete Lyapunov and long-time convergence; the Kalman cycle has a separate augmented plant–estimator check reported in the audit data.
7. Secular-RWA and full bare-local CP thresholds are compared without identifying their distinct reservoir conventions.
8. Every accepted covariance passes $\sigma + i\boldsymbol{\Omega}/2 \geq 0$ after rescaling.
9. Gravity-off local feedback gives zero unconditional negativity.
10. Weak gravity uses 60-digit arithmetic; double-precision zero is never reported as proof.

E Reproducibility inventory

The authoritative scripts are grouped by function:

- covariance core: `code/gmec_core.py`, `code/gmec_dynamics.py` and `code/gmec_protocols.py`;
- audits: `code/gmec_static_audit.py`, `code/gmec_geometry_audit.py`, `code/gmec_modulation_audit.py`, `code/gmec_cp_periodic_recheck.py` and the Kalman scripts, including `code/gmec_feedback_thresholds.py` and `code/gmec_kalman_periodic_independent.py`;
- outputs: `code/gmec_protocol_search.py` and `code/gmec_generate_figures.py`.

Generated data live in `data/`; manuscript figures live in `figures/`. Python uses NumPy, SciPy, mpmath and Matplotlib. The report is built with `latexmk`, `pdflatex` and `biber`. From the repository root, run `PYTHONPATH=codepythoncode/gmec_cp_periodic_recheck.py` and `PYTHONPATH=codepythoncode/gmec_generate_figures.py`; then run `make` in the manuscript directory.

F Claim-status index

Exact algebraic statements within the quadratic model are labelled Proof; computed values and finite-grid searches are Numerical result; extrapolations controlled by a dimensionless limit are Scaling argument; and experimental or beyond-model proposals are Conjecture. A numerical search is never promoted to a no-go proof.

Data availability statement

All source code, generated tables and figures used in this report are included in the project repository. No external experimental dataset is analysed.

Ethics declaration

This is a theoretical and computational study with no human participants, animals or sensitive personal data.

Author contributions

Heah Hung Xun: conceptualisation, methodology, software, validation, formal analysis, visualisation and writing. AI-assisted research tools were used for algebraic checking, code generation, literature retrieval and editorial review; all reported conclusions were recomputed and reconciled against independent routes.

Conflict of interest

The author declares no conflict of interest.

Funding

No specific funding is declared in this report.

References

[1] R. Simon. "Peres-Horodecki Separability Criterion for Continuous Variable Systems". In: *Physical Review Letters* 84 (2000), p. 2726. DOI: 10.1103/PhysRevLett.84.2726. arXiv: quant-ph/9909044.

[2] G. Vidal and R. F. Werner. "Computable measure of entanglement". In: *Physical Review A* 65 (2002), p. 032314. DOI: 10.1103/PhysRevA.65.032314. arXiv: quant-ph/0102117.

[3] Alexander N. Poddubny et al. "Nonequilibrium Entanglement between Levitated Masses under Optimal Control". In: *arXiv preprint* (2025). arXiv: 2408.06251 [quant-ph].

[4] Klemens Winkler et al. "Steady-State Entanglement of Interacting Masses in Free Space through Optimal Feedback Control". In: *Physical Review Research* (2025). DOI: 10.1103/hxc8-fxcb. arXiv: 2408.07492.

[5] Ankit Kumar et al. "Continuous-Variable Entanglement through Central Forces: Application to Gravity between Quantum Masses". In: *Quantum* 7 (2023), p. 1008. arXiv: 2206.12897.

[6] Ankit Kumar and Tomasz Paterek. "Parametric Modulation of Gravitational Entanglement". 2024.

[7] Dvir Kafri, Jacob M. Taylor, and Gerard J. Milburn. "A classical channel model for gravitational decoherence". In: *New Journal of Physics* 16 (2014), p. 065020. DOI: 10.1088/1367-2630/16/6/065020. arXiv: 1401.0946.

[8] Samuel Schlegel et al. "Gravitational Entanglement in Optomechanics: Distinguishing Classical and Quantum Models". In: *arXiv preprint* (2026). arXiv: 2605.20330 [quant-ph].